

# Structural and electronic properties of AuIr nanoalloys<sup>\*</sup>

Laura M. Jiménez-Díaz and Luis A. Pérez<sup>a</sup>

Instituto de Física, Universidad Nacional Autónoma de México, Apartado Postal 20-364, 01000 México, D. F., México

Received 29 August 2012 / Received in final form 27 November 2012

Published online 5 February 2013 – © EDP Sciences, Società Italiana di Fisica, Springer-Verlag 2013

**Abstract.** The lowest-energy structures of binary  $(\text{AuIr})_n$ ,  $(\text{AuIr}_3)_s$ , and  $(\text{Au}_3\text{Ir})_s$  clusters, with  $n = 2-20$ , and  $s = 5$ , modeled by the many-body Gupta potential, were obtained by using a genetic-symbiotic algorithm. These structures were further relaxed within the density functional theory to obtain the most stable structures for each composition. Segregation is observed in all the AuIr clusters, where the Ir atoms occupy the cluster core and the Au atoms are situated on the cluster surface. On the other hand, there is experimental evidence that the  $(\text{AuIr})_n$  nanoalloys could have an enhanced catalytic activity for CO oxidation. In order to study this phenomenon, we also performed first-principles density functional calculations of the CO and O<sub>2</sub> adsorption on these bimetallic nanoclusters, considering three different compositions and a fixed cluster size of 20 atoms.

## 1 Introduction

It is known that the physical and chemical properties of bimetallic clusters or nanoalloys, composed of two metal elements, may be tuned by varying not only their size and geometries, but also their composition [1,2] and, in many cases, they have enhanced catalytic properties as compared with the corresponding monometallic clusters [3]. On the other hand, the CO oxidation on supported nanogold catalysts has been a subject of intensive study during the last years. In particular, it has been found that the catalytic activity of Au nanoparticles supported on reducible oxides (such as TiO<sub>2</sub> and Fe<sub>2</sub>O<sub>3</sub>) is at least one order of magnitude greater than that of Au supported on inert substrates (e.g., MgO, SiO<sub>2</sub>) under similar conditions [4]. However, these gold catalysts are not stable because their catalytic activity decreases with time due to either the sintering of gold nanoparticles or to the adsorption of carbonates on catalytic active sites [5]. Okumura et al. [6] found that adding Ir to Au/TiO<sub>2</sub> catalysts enhance their catalytic activity for oxidative reactions at high temperatures such as the decomposition of dyoxin. Moreover, codepositing Au and Ir on rutile (TiO<sub>2</sub>) single crystal, can produce Au particles (5–10 nm) which epitaxially cap IrO<sub>2</sub> pillars dispersed on the TiO<sub>2</sub> [7]. Density functional studies of the latter system show that the presence of IrO<sub>2</sub> produces an active Au/IrO<sub>2</sub> interface while preserving the resistance to sintering of the gold particles [8]. More recent studies also show that the addition of iridium to Au/TiO<sub>2</sub> catalysts, stabilize them against sintering and improves

their catalytic activity for CO oxidation [9]. Furthermore, it has been found that Ir-Au/rutile catalysts have small iridium particles containing gold and having dimensions of the order of 1 nm and, probably, these nanoparticles are responsible for the enhancement of the activity of these catalysts for the CO oxidation [10]. Since there is experimental evidence that supported AuIr nanoparticles can be formed, in this work we present a density functional study of the structural and electronic properties of the gas phase  $(\text{AuIr})_n$ ,  $(\text{Au}_3\text{Ir})_s$  and  $(\text{AuIr}_3)_s$  ( $n = 2-20$ ,  $s = 5$ ) atomic clusters, within the generalized gradient approximation (GGA). In order to have some insight on the possible catalytic activity of these nanoalloys for the CO oxidation, we also address the molecular CO and O<sub>2</sub> adsorption on gas-phase  $\text{Au}_m\text{Ir}_n$  clusters with  $m + n = 20$ , and  $m = 3n$ ,  $m = n$  and  $n = 3m$ .

## 2 Theoretical methodology

In the initial stage of our study, a distribution of the lowest-energy isomers of the AuIr bimetallic clusters (with a given size and composition) is obtained by performing global optimizations using the Gupta many-body potential [11] and a generalized version of the genetic-symbiotic algorithm by Michaelian et al. [12,13]. The Gupta parameters were taken from reference [11] for the Au-Au and Ir-Ir interactions. In the case of Au-Ir interactions, a geometrical average of the Au-Au and Ir-Ir interactions was taken for the  $A$  and  $\zeta$  parameters of the Gupta potential, whereas an arithmetic average was used for the  $p$ ,  $q$ , and  $r_0$  parameters. In the second stage, some of the more relevant isomers of this distribution (typically ten) were used as initial configurations in a further local structural reoptimization with an unconstrained

<sup>\*</sup> ISSPIC 16 - 16th International Symposium on Small Particles and Inorganic Clusters, edited by Kristiaan Temst, Margriet J. Van Bael, Ewald Janssens, H.-G. Boyen and Françoise Remacle.

<sup>a</sup> e-mail: lperez@fisica.unam.mx

conjugate gradient (CG) procedure, using the forces obtained from a DFT-GGA calculation within the PBE parametrization [14]. This approach has been used in previous studies of monometallic [15] and bimetallic clusters [16–19] showing an evident effectiveness. We used the DFT code SIESTA [20] with standard norm-conserving pseudopotentials [21] in their fully nonlocal form [22]. These pseudopotentials were generated with the atomic valence-electron configurations  $d^{10}s^1$  (Au),  $d^7s^2$  (Ir),  $s^2p^2$  (C) and  $s^2p^4$  (O). The core radii (in atomic units) are as follows:  $s$  (2.32),  $p$  (2.32),  $d$  (2.32) for Au;  $s$  (2.60),  $p$  (2.77),  $d$  (2.60) for Ir;  $s$  (1.14),  $p$  (1.14),  $d$  (1.14) for O; and  $s$  (1.25),  $p$  (1.25),  $d$  (1.25) for C. We used double- $\zeta$   $s$ ,  $d$ -basis and single  $p$  polarization orbitals, whereas, for C and O we used a double- $\zeta$   $s$ ,  $p$ -basis and single  $d$  orbitals. We also used an energy cutoff of 150 Ry to define the real space grid for numerical integrations. All the calculations included spin polarization. The clusters were let free to relax until the Hellmann-Feynman forces were less than 20 meV/Å. Likewise, the lowest-energy configurations of the  $\text{Au}_m\text{Ir}_n\text{CO}$ ,  $\text{Au}_m\text{Ir}_n\text{O}_2$  and  $\text{Au}_m\text{Ir}_n\text{O}_2\text{CO}$  complexes were also found by performing CG structural relaxations using the DFT forces, starting with the lowest-energy isomers of the  $\text{Au}_m\text{Ir}_n$  clusters previously obtained, and testing several different initial positions (typically 20) for the adsorbed CO and O<sub>2</sub> molecules on the bimetallic cluster. For the metal dimers the following bond distances and binding energies were obtained: (2.526 Å, 2.778 eV) for Au<sub>2</sub> and (2.349 Å, 4.483 eV) for Ir<sub>2</sub>. The suitability of the double zeta polarized (DZP) basis set has been tested by comparing the calculated bond lengths of the Au and Ir dimers with those obtained with the GPAW package [23,24], which uses a uniform real-space grid representation of the electronic wave functions. These values are 2.557 Å and 2.264 Å for Au<sub>2</sub> and Ir<sub>2</sub>, respectively, and they are in good agreement with the DZP ones. The experimental values for neutral dimers are [25]: (2.47 Å, 2.29 ± 0.02 eV) for Au<sub>2</sub> and (2.27 Å, 3.7 ± 0.7 eV) for Ir<sub>2</sub>. It is well known the relatively high error of current xc-approximations in the calculated values of binding energies with respect to experiments.

### 3 Physical properties of AuIr clusters

The lowest-energy isomers obtained for  $(\text{AuIr})_n$ , with  $n = 2–20$ , are shown in Figure 1. Observe that for  $n = 2$  and  $n = 3$ , nearly planar structures are found with the Ir atoms at the center and the Au atoms at the extremes. Almost all the structures are amorphous and many of them present decahedral motifs except for  $n = 17, 18$  and 19, where fcc-like structures are found. In particular, for  $n = 19$ , the structure of the most stable isomer is a distorted cube-octahedron. It is worth mentioning that the same geometry is found for the  $(\text{PtPd})_{19}$  and  $(\text{PtNi})_{19}$  lowest-energy isomers [16,19]. The general trend observed in the  $(\text{AuIr})_n$  lowest-energy isomers is that their structures are characterized by a segregation phenomenon, where the Ir atoms form the cluster core whereas the

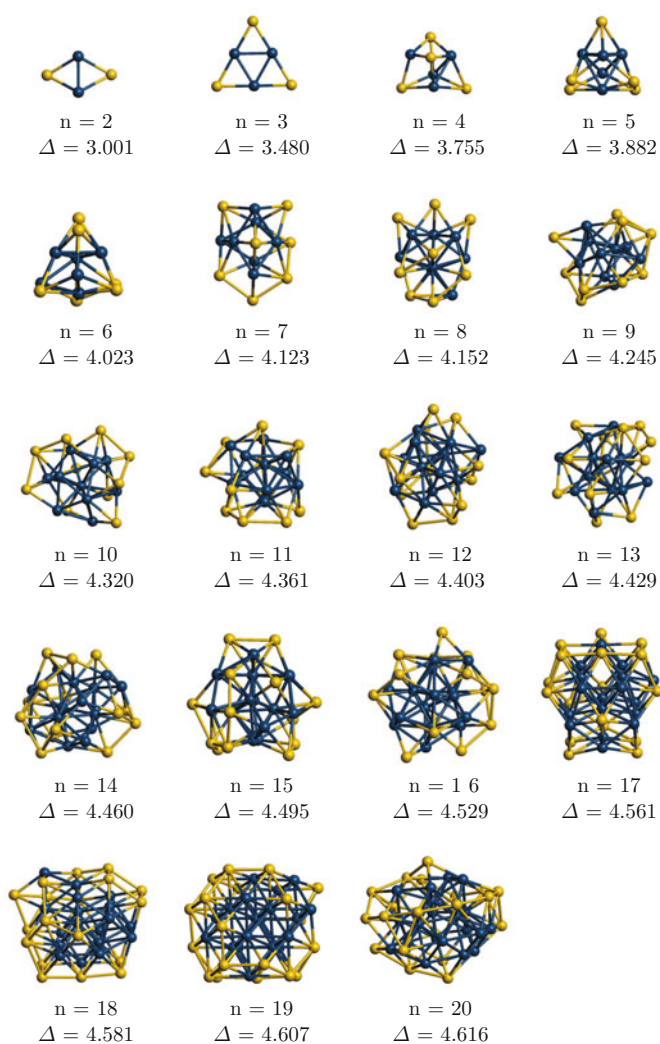


**Fig. 1.** Geometric structures and binding energies per atom ( $\Delta$ ) in eV for the most stable isomers of  $(\text{AuIr})_n$ , with  $n = 2–20$ . The blue spheres represent the Ir atoms.

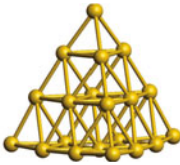
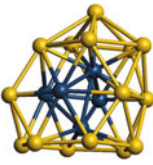
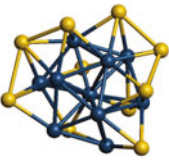
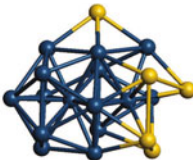
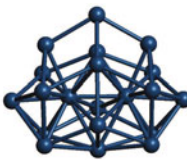
Au atoms are situated on the cluster surface. This phenomenon is due to the higher binding energy of Ir atoms in comparison to that of Au atoms, and it can be observed by inspection of the corresponding structures or by calculating the interatomic mean distance given by:

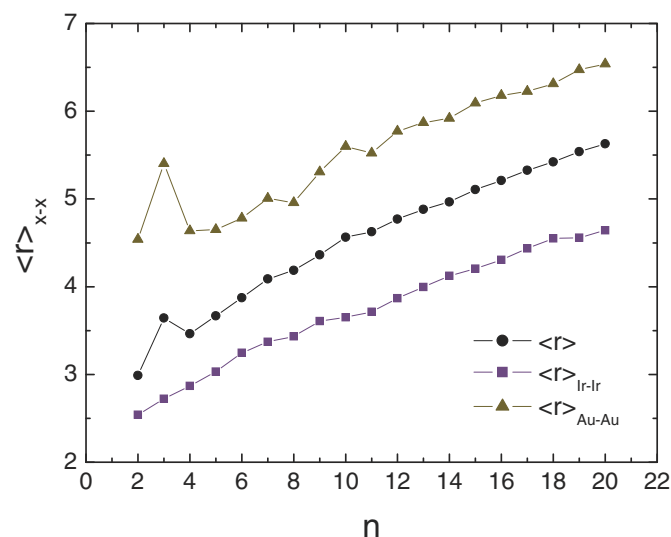
$$\langle r \rangle_{x-x} = \frac{1}{N_x} \sum_{i < j}^{N_x} |\mathbf{r}_{x_i} - \mathbf{r}_{x_j}|, \quad (1)$$

where  $x_i$  denotes  $i$ -atom of species  $x$  (Au, Ir) and  $N_x$  is the number of atoms of species  $x$ . In Figure 2,  $\langle r \rangle_{\text{Au-Au}}$  (solid triangles),  $\langle r \rangle_{\text{Ir-Ir}}$  (solid squares), and  $\langle r \rangle$  (solid circles) are shown as a function of  $n$  for  $(\text{AuIr})_n$  clusters. Here,  $\langle r \rangle$  denotes the atomic mean distance without distinguishing between species.

Notice that  $\langle r \rangle_{\text{Ir-Ir}}$  is always smaller than  $\langle r \rangle_{\text{Au-Au}}$  for all the values of  $n$  considered, indicating that, for a given cluster, the Ir atoms form a more compact structure than that of the Au atoms. In particular,  $\langle r \rangle_{\text{Au-Au}}(n)$  shows a peak for  $n = 3$  since the corresponding structure

**Table 1.** Geometric structures, binding energies per atom (in eV) and interatomic mean distances (in Å) for the most stable isomers of Au<sub>20</sub>, Au<sub>15</sub>Ir<sub>5</sub>, Au<sub>10</sub>Ir<sub>10</sub>, Au<sub>5</sub>Ir<sub>15</sub>, and Ir<sub>20</sub>. Yellow and blue spheres represent Au and Ir atoms, respectively.

| Au <sub>20</sub>  | Au <sub>15</sub> Ir <sub>5</sub>  | Au <sub>10</sub> Ir <sub>10</sub>   | Au <sub>5</sub> Ir <sub>15</sub>   | Ir <sub>20</sub>  |
|---|---|---|--|---|
|  |  |  |  |  |
| $\Delta = 3.008$  | $\Delta = 3.647$  | $\Delta = 4.320$  | $\Delta = 4.891$   | $\Delta = 5.443$  |
| $\langle r \rangle = 4.815$   | $\langle r \rangle = 4.500$   | $\langle r \rangle = 4.565$   | $\langle r \rangle = 4.448$  | $\langle r \rangle = 4.410$   |
|   | $\langle r \rangle_{\text{Ir-Ir}} = 3.123$  | $\langle r \rangle_{\text{Ir-Ir}} = 3.651$  | $\langle r \rangle_{\text{Ir-Ir}} = 4.034$   |   |
|   | $\langle r \rangle_{\text{Au-Au}} = 4.974$  | $\langle r \rangle_{\text{Au-Au}} = 5.597$  | $\langle r \rangle_{\text{Au-Au}} = 4.547$   |   |

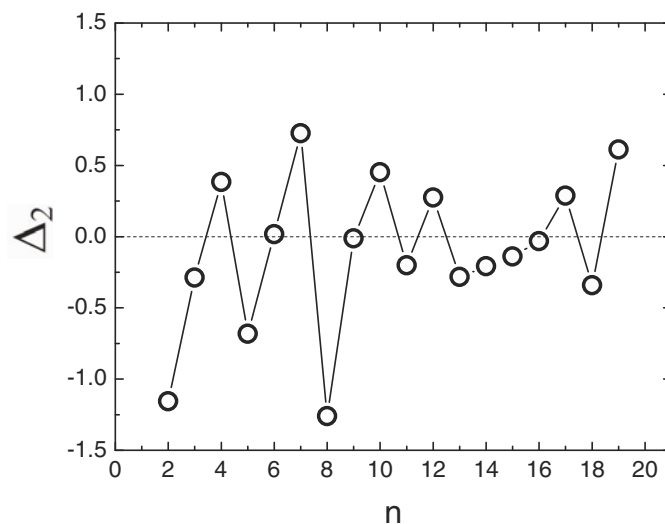
**Fig. 2.** Interatomic mean distances versus  $n$  for the lowest-energy  $(\text{AuIr})_n$  ( $n = 2$ – $20$ ) isomers.

is an equilateral triangle with the Au atoms occupying the three distant corners. On the other hand, it should be mentioned the existence of cluster sizes with special stability with respect to smaller or larger sizes. This kind of “magic number” cluster sizes can be identified by calculating a second difference ( $\Delta_2$ ) in the cluster energy between size-neighboring clusters for a given composition. For the case of  $(\text{AuIr})_n$  bimetallic clusters, we calculated

$$\Delta_2(n) = E(n+1) + E(n-1) - 2E(n). \quad (2)$$

This quantity is shown in Figure 3 for  $(\text{AuIr})_n$  clusters where the peaks at  $n = 7, 19, 10$  and  $4$  indicate a higher stability of these cluster sizes with respect to other ones.

Table 1 shows the lowest-energy isomers of 20-atom Au<sub>10</sub>Ir<sub>10</sub>, Au<sub>5</sub>Ir<sub>15</sub> and Au<sub>15</sub>Ir<sub>5</sub> nanoalloys, as well as those of Ir<sub>20</sub> and Au<sub>20</sub> monoatomic clusters as reference. It is worth mentioning that our calculations also confirm that the most stable Au<sub>20</sub> isomer in gas phase is the tetrahedral structure discovered by Li et al. [26]. For the three compositions of the 20-atom AuIr nanoalloys considered, the Ir atoms also tend to occupy the cluster core whereas

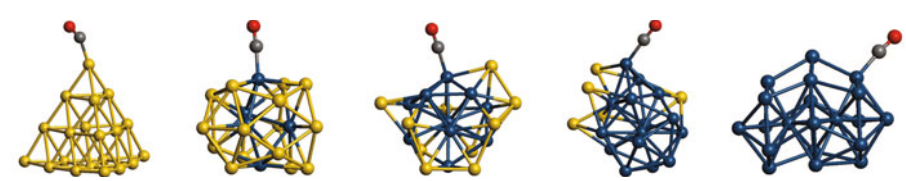
**Fig. 3.** Second difference in the energy [ $\Delta_2(n)$ ] versus cluster size for  $(\text{AuIr})_n$  most stable isomers.

the Au atoms tend to occupy the cluster surface since  $\langle r \rangle_{\text{Au-Au}} > \langle r \rangle > \langle r \rangle_{\text{Ir-Ir}}$ . Notice also that the 20-atom cluster binding energy increases monotonically when the Ir content augments from zero to 20, as expected. Besides,  $\langle r \rangle$  indicates that the Ir<sub>20</sub> cluster has the most compact structure of the most stable 20-atom Au<sub>*m*</sub>Ir<sub>*n*</sub> clusters, whereas the Au<sub>20</sub> cluster is the less compact one. Furthermore, the mean distance between Ir atoms increases monotonically when their number augments for a fixed Au<sub>*m*</sub>Ir<sub>*n*</sub> cluster size, while the mean distance between Au atoms shows a non-monotonic behavior. Due to this, the overall interatomic mean distance  $\langle r \rangle$  of the 20-atom AuIr clusters also show a non-monotonic behavior as a function of the Ir content.

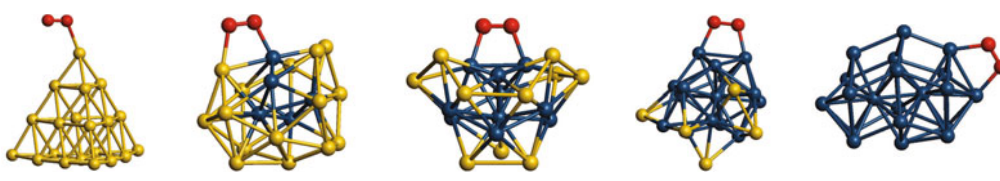
#### 4 Adsorption of CO and O<sub>2</sub> on AuIr clusters

Tables 2 and 3, respectively, show the most stable configurations of molecular CO and O<sub>2</sub> adsorbed on the lowest-energy Au<sub>*m*</sub>Ir<sub>*n*</sub> ( $m+n=20$ ,  $m, n=0, 5, 10, 15, 20$ )

**Table 2.** Lowest-energy configurations of molecular CO adsorbed on the most stable  $\text{Au}_m\text{Ir}_n$  clusters together with CO adsorption energies, charge transfers and C-O bond distances. The corresponding data for  $\text{Au}_{20}\text{CO}$  and  $\text{Ir}_{20}\text{CO}$  are also included. Yellow, blue, red and grey spheres represent Au, Ir, O and C atoms, respectively.

|  | $\text{Au}_{20}\text{CO}$ | $\text{Au}_{15}\text{Ir}_5\text{CO}$ | $\text{Au}_{10}\text{Ir}_{10}\text{CO}$ | $\text{Au}_5\text{Ir}_{15}\text{CO}$ | $\text{Ir}_{20}\text{CO}$ |
|--|---------------------------|--------------------------------------|---|--------------------------------------|---------------------------|
|  |                           |                                      |   |                                      |                           |
| $E_{\text{ads}}$ [eV]  | 1.298                     | 2.441                                | 2.441                                   | 2.698                                | 2.849                     |
| $\Delta q$   | -0.026                    | 0.122                                | 0.133                                   | 0.159                                | 0.184                     |
| $d_{\text{C-O}}$ [Å]   | 1.176                     | 1.196                                | 1.197                                   | 1.200                                | 1.203                     |

**Table 3.** Lowest-energy configurations of molecular  $\text{O}_2$  adsorbed on the most stable  $\text{Au}_m\text{Ir}_n$  clusters together with  $\text{O}_2$  adsorption energies, charge transfers and O-O bond distances. The corresponding data for  $\text{Au}_{20}\text{O}_2$  and  $\text{Ir}_{20}\text{O}_2$  are also included. Yellow, blue and red spheres represent Au, Ir and O atoms, respectively.

|   | $\text{Au}_{20}\text{O}_2$ | $\text{Au}_{15}\text{Ir}_5\text{O}_2$ | $\text{Au}_{10}\text{Ir}_{10}\text{O}_2$ | $\text{Au}_5\text{Ir}_{15}\text{O}_2$ | $\text{Ir}_{20}\text{O}_2$ |
|---|----------------------------|---------------------------------------|--|---------------------------------------|----------------------------|
|  |                            |                                       |  |                                       |                            |
| $E_{\text{ads}}$ [eV]   | 0.430                      | 1.287                                 | 1.862                                    | 2.438                                 | 2.449                      |
| $\Delta q$  | 0.068                      | 0.266                                 | 0.323                                    | 0.410                                 | 0.418                      |
| $d_{\text{O-O}}$ [Å]  | 1.259                      | 1.336                                 | 1.364                                    | 1.404                                 | 1.396                      |

clusters, as well as the corresponding CO ( $\text{O}_2$ ) adsorption energies ( $E_{\text{ads}}$ ), excess electronic charges ( $\Delta q$ ) on the molecular CO ( $\text{O}_2$ ), and the C-O (O-O) bond distances.  $E_{\text{ads}}$  is calculated from:

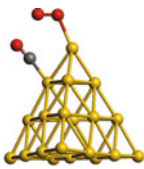
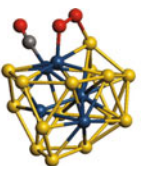
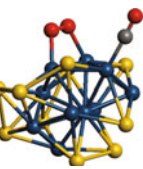
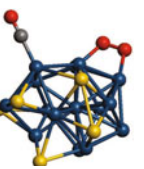
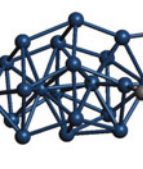
$$E_{\text{ads}} = E(\text{Au}_m\text{Ir}_n) + E(\text{Y}) - E(\text{Au}_m\text{Ir}_n\text{Y}), \quad (3)$$

where  $E(X)$  is the total energy of system X, and Y denotes the CO or  $\text{O}_2$  molecule. The excess electronic charges  $\Delta q$  are obtained from a Mulliken population analysis. Notice that the CO always binds through the C atom to an Ir atom of the  $\text{Au}_m\text{Ir}_n$  nanoalloys in a top configuration. The same configuration is found for the CO adsorbed onto the  $\text{Au}_{20}$  and  $\text{Ir}_{20}$  clusters. The greatest CO adsorption energy is found for  $\text{Ir}_{20}$  and it decreases when the Au content increases, being nearly the same for  $m = 15$ ,  $n = 5$  and  $m = n = 10$ , until it reaches its minimum value for  $m = 20$ ,  $n = 0$ . For the latter case, the CO adsorption energy is nearly half of the values found for the studied 20-atom AuIr nanoalloys. In the three 20-atom AuIr nanoalloys analyzed together with the  $\text{Ir}_{20}$  cluster, electronic charge is transferred from the bimetallic cluster to the CO, being greater when the CO adsorbs on the pure Ir cluster. This charge excess on the CO molecule decreases when the Au content in the cluster augments until that, for the case of  $\text{Au}_{20}$ , a slight charge transfer from the CO to the cluster is found. As expected, the C-O bond distance increases with respect to the one calculated

for the free CO molecule (1.17 Å) when  $\Delta q$  grows. On the other hand, the greatest  $\text{O}_2$  adsorption energy is found for  $\text{Ir}_{20}$ , and it decreases when the Au concentration increases for a fixed 20-atom cluster size, being almost the same for  $m = 0$ ,  $n = 20$  and  $m = 5$ ,  $n = 15$ , until it reaches a value of 0.43 eV for  $\text{Au}_{20}$ , where the  $\text{O}_2$  binds to a corner of the gold tetrahedron in a top configuration. Except for the case of  $\text{Au}_{20}$ , the most stable  $\text{O}_2$  adsorbed configurations onto  $\text{Au}_m\text{Ir}_n$  clusters correspond to the two O atoms bound to two Ir atoms in a staple-like configuration ( $m = 10$ ,  $n = 10$ ;  $m = 5$ ,  $n = 15$ ;  $m = 0$ ,  $n = 20$ ), or bound to one Ir atom and one Au atom also in a staple-like geometry ( $m = 15$ ,  $n = 5$ ). For the three 20-atom AuIr nanoalloys studied together with the  $\text{Ir}_{20}$  and  $\text{Au}_{20}$  clusters, there is charge transfer from the cluster to the  $\text{O}_2$  adsorbed molecule, being greater for the pure Ir cluster and lesser for the pure Au cluster. The charge transfer from the cluster to the  $\text{O}_2$  molecule weakens the O-O bond and its length grows with  $\Delta q$ , being larger than the calculated value for the free  $\text{O}_2$  molecule (1.24 Å). Moreover,  $\Delta q$  also grows when the corresponding adsorption energy increases and its values are much larger than those corresponding to the CO molecule and to that calculated for the  $\text{Au}_{20}\text{O}_2$  complex.

Table 4 shows the most stable configurations of a CO molecule and a  $\text{O}_2$  molecule coadsorbed on the lowest-energy  $\text{Au}_m\text{Ir}_n$  ( $m + n = 20$ ,  $m, n = 0, 5, 10, 15$ ) isomers.

**Table 4.** Lowest-energy configurations of CO and O<sub>2</sub> coadsorbed on the most stable Au<sub>m</sub>Ir<sub>n</sub> clusters together with CO (O<sub>2</sub>) adsorption energies, charge transfers and C-O (O-O) bond distances. The corresponding data for Au<sub>20</sub>O<sub>2</sub>CO and Ir<sub>20</sub>O<sub>2</sub>CO are also included. Yellow, blue, red and grey spheres represent Au, Ir, O and C atoms, respectively.

|   | Au <sub>20</sub> O <sub>2</sub> CO  | Au <sub>15</sub> Ir <sub>5</sub> O <sub>2</sub> CO                                | Au <sub>10</sub> Ir <sub>10</sub> O <sub>2</sub> CO                                | Au <sub>5</sub> Ir <sub>15</sub> O <sub>2</sub> CO                                  | Ir <sub>20</sub> O <sub>2</sub> CO |
|---|---|---|--|---|------------------------------------|
|  |  |  |  |  |                                    |
| $E_{\text{ads}}^{\text{CO}}$ [eV]   | 1.015   | 2.379   | 2.278  | 2.571   | 2.587                              |
| $\Delta q^{\text{CO}}$  | -0.013  | 0.113   | 0.114  | 0.148   | 0.180                              |
| $d_{\text{C-O}}$ [Å]  | 1.178   | 1.194   | 1.191  | 1.200   | 1.202                              |
| $E_{\text{ads}}^{\text{O}_2}$ [eV]  | 0.481   | 1.225   | 1.699  | 2.312   | 2.405                              |
| $\Delta q^{\text{O}_2}$   | 0.094   | 0.272   | 0.306  | 0.388   | 0.409                              |
| $d_{\text{O-O}}$ [Å]  | 1.262   | 1.332   | 1.360  | 1.396   | 1.398                              |

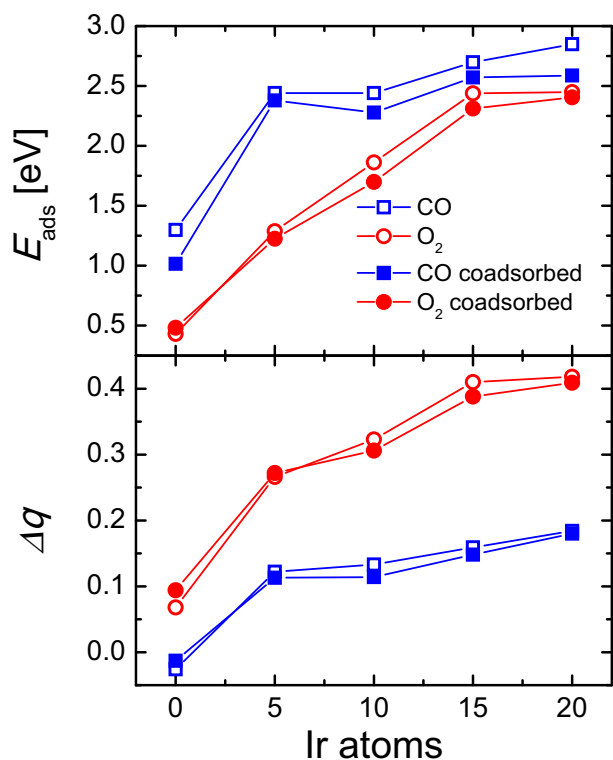


**Fig. 4.** Adsorption energies ( $E_{\text{ads}}$ ) and excess electronic charges ( $\Delta q$ ) for molecular CO and O<sub>2</sub> on the most stable 20-atom AuIr clusters versus number of Ir atoms.

The adsorption energy  $E_{\text{ads}}^{\text{X}}$  of molecule X was calculated as:

$$E_{\text{ads}}^{\text{X}} = E(\text{Au}_m\text{Ir}_n\text{Y}) + E(\text{X}) - E(\text{Au}_m\text{Ir}_n\text{XY}), \quad (4)$$

where X and Y are the two coadsorbed molecules (X, Y = CO, O<sub>2</sub>). In contrast to the single-molecule adsorption case, the adsorption energies for the coadsorbed CO show a non-monotonic behavior as a function of the Ir concentration, where  $E_{\text{ads}}^{\text{CO}}$  on Au<sub>15</sub>Ir<sub>5</sub>O<sub>2</sub> is slightly larger than

the corresponding energy for CO on Au<sub>10</sub>Ir<sub>10</sub>O<sub>2</sub>. However, in general, the adsorption energies for the coadsorbed CO and O<sub>2</sub> increase with the Ir content and they are lower than the corresponding single-molecule adsorption energies. On the other hand, the charge transfers from the bimetallic cluster to the two coadsorbed molecules also increases with the Ir content, being greater for the O<sub>2</sub> than for CO. Figure 4 summarizes the results for molecular adsorption energies and charge transfers, for both single-molecule adsorption and coadsorption cases, as a function of the Ir content for the 20-atom Au<sub>m</sub>Ir<sub>n</sub> ( $m+n=20$ ,  $m, n=0, 5, 10, 15$ ) most stable clusters. Notice that the charge transfer from the cluster to the O<sub>2</sub> molecule is always larger than the corresponding charge transfer to the CO, suggesting that the addition of Ir to Au nanoclusters could enhance the dissociation of O<sub>2</sub>.

## 5 Summary

In this paper, the structural and electronic properties of gas-phase (AuIr)<sub>n</sub>, (AuIr<sub>3</sub>)<sub>s</sub>, and (Au<sub>3</sub>Ir)<sub>s</sub> nanoclusters, with  $n=2-20$  and  $s=5$ , were investigated within the DFT-GGA framework. Segregation is found for all the studied AuIr clusters where the Ir atoms are concentrated in the cluster core and the Au atoms are situated on the cluster surface. This phenomenon is due to the higher binding energy of the Ir atoms in comparison to that of Au atoms. It is worth mentioning that the truncated cubooctahedral geometry adopted by the most stable (AuIr)<sub>19</sub> isomer is also found for the lowest-energy (PtPd)<sub>19</sub> and (PtNi)<sub>19</sub> isomers. Moreover, for a fixed cluster size of 20 atoms, we also studied the adsorption and coadsorption of CO and O<sub>2</sub> on the most stable Au<sub>m</sub>Ir<sub>n</sub> ( $m+n=20$ ,  $m, n=0, 5, 10, 15, 20$ ) isomers, including the cases of Au<sub>20</sub> and Ir<sub>20</sub> as reference. Except for the Au<sub>20</sub>CO complex, there is always charge transfer from the cluster to the CO and O<sub>2</sub> molecules, being greater for the pure Ir cluster and it decreases when the

Au content augments. A similar trend is found for the molecule (CO or O<sub>2</sub>) adsorption energy, where the greatest value corresponds to the pure Ir cluster and it diminishes when the Au content in the cluster increases. Since a high value of the charge transfer from the cluster to the O<sub>2</sub> molecule enhance its decomposition, but also a high adsorption energy could hinder its subsequent release, the results suggest that adding Au atoms to Ir nanoclusters can diminish their huge O<sub>2</sub> adsorption energy and still conserving a charge transfer to the molecule.

This work was supported by DGAPA-UNAM under Grant IN102511. Computations were done at supercomputer Kan-Balam of DGTIC-UNAM. L.M. Jiménez-Díaz acknowledges CONACyT scholarship.

## References

1. J. Jellinek, E.B. Krissinel, *Theory of Atomic and Molecular Clusters*, edited by J. Jellinek (Springer, Berlin, 1999)
2. R. Ferrando, J. Jellinek, R.L. Johnston, *Chem. Rev.* **108**, 845 (2008)
3. J.H. Sinfelt, *Bimetallic Catalysts: Discoveries, Concepts and Applications* (Wiley, New York, 1983)
4. M.M. Schubert, S. Hackenberg, A.C. van Veen, M. Muhler, V. Plzak, R.J. Behm, *J. Catal.* **197**, 113 (2001)
5. T.V. Choudhary, D.W. Goodman, *Top. Catal.* **21**, 25 (2002)
6. M. Okumura, T. Akita, M. Haruta, X. Wang, O. Kajikawa, O. Okada, *J. Appl. Catal. B* **41**, 43 (2003)
7. T. Akita, M. Okumura, K. Tanaka, S. Tsubota, M. Haruta, *J. Electron Microsc.* **52**, 119 (2003)
8. Z.-P. Liu, S.J. Jenkins, D.A. King, *Phys. Rev. Lett.* **93**, 156102 (2004)
9. A. Gómez-Cortés, G. Díaz, R. Zanella, H. Rodríguez, P. Santiago, J.M. Saniger, *J. Phys. Chem. C* **113**, 9719 (2009)
10. X. Bokhimi, R. Zanella, C. Angeles-Chavez, *J. Phys. Chem. C* **114**, 14101 (2010)
11. F. Cleri, V. Rosato, *Phys. Rev. B* **48**, 22 (1993)
12. K. Michaelian, *Chem. Phys. Lett.* **293**, 202 (1998)
13. K. Michaelian, N. Rendón, I.L. Garzón, *Phys. Rev. B* **60**, 2000 (1999)
14. J.P. Perdew, K. Burke, M. Ernzerhof, *Phys. Rev. Lett.* **77**, 3865 (1996)
15. I.L. Garzón, M.R. Beltrán, G. González, I. Gutiérrez-González, K. Michaelian, J.A. Reyes-Nava, J.I. Rodríguez-Hernández, *Eur. Phys. J. D* **24**, 105 (2003)
16. E.M. Fernández, L.C. Balbás, L.A. Pérez, K. Michaelian, I.L. Garzón, *Int. J. Mod. Phys. B* **19**, 2339 (2005)
17. L.O. Paz-Borbón, A. Gupta, R.L. Johnston, *J. Mater. Chem.* **18**, 4154 (2008)
18. R. Ferrando, A. Fortunelli, R.L. Johnston, *Phys. Chem. Chem. Phys.* **10**, 640 (2008)
19. A. Radillo-Díaz, Y. Coronado, L.A. Pérez, I.L. Garzón, *Eur. Phys. J. D* **52**, 127 (2009)
20. J.M. Soler et al., *J. Phys.: Condens. Matter* **14**, 2745 (2002)
21. N. Troullier, J.L. Martins, *Phys. Rev. B* **43**, 1993 (1991)
22. L. Kleinman, D.M. Bylander, *Phys. Rev. Lett.* **48**, 1425 (1982)
23. J.J. Mortensen, L.B. Hansen, K.W. Jacobsen, *Phys. Rev. B* **71**, 035109 (2005)
24. J. Enkovaara et al., *J. Phys.: Condens. Matter* **22**, 253202 (2010)
25. M.D. Morse, *Chem. Rev.* **86**, 1049 (1986)
26. J. Li, X. Li, H.-J. Zhai, L.-S. Wang, *Science* **299**, 864 (2003)